IOPscience iopscience.iop.org

Home Search Collections Journals About Contact us My IOPscience

Spin dynamics in a compound semiconductor spintronic structure with a Schottky barrier

This article has been downloaded from IOPscience. Please scroll down to see the full text article.

2006 J. Phys.: Condens. Matter 18 1535

(http://iopscience.iop.org/0953-8984/18/5/005)

View the table of contents for this issue, or go to the journal homepage for more

Download details:
IP Address: 129.252.86.83
The article was downloaded on 28/05/2010 at 08:53

Please note that terms and conditions apply.

INSTITUTE OF PHYSICS PUBLISHING JOURNAL OF PHYSICS: CONDENSED MATTER

J. Phys.: Condens. Matter **18** (2006) 1535–1544 doi:10.1088/0953-8984/18/5/005

Spin dynamics in a compound semiconductor spintronic structure with a Schottky barrier

Semion Saikin[1,2,3], **Min Shen**[1] **and Ming-Cheng Cheng**[1]

[1] Center for Quantum Device Technology, Department of Electrical and Computer Engineering, Clarkson University, Potsdam, NY 13699, USA
[2] Department of Physics, Kazan State University, Kazan, 420008, Russian Federation

Received 15 September 2005, in final form 24 November 2005
Published 17 January 2006
Online at stacks.iop.org/JPhysCM/18/1535

Abstract

We demonstrate theoretically that spin dynamics of electrons injected into a GaAs semiconductor structure through a Schottky barrier possesses strong non-equilibrium features. The electrons injected are redistributed quickly among several valleys. Spin relaxation driven by the spin–orbital coupling in the semiconductor is very rapid. At $T = 4.2$ K, injected spin polarization decays at a distance of the order of 50–100 nm from the interface. This spin penetration depth reduces approximately by half at room temperature. The spin scattering length is different for different valleys.

1. Introduction

Electrical spin injection into a non-magnetic semiconductor structure is one of the most complicated issues in the design of semiconductor spintronic devices [1–3]. A high efficiency of spin injection in magnetic/non-magnetic semiconductor structures has been demonstrated in the diffusive transport regime [4]. Also, in the ballistic transport regime, spin filtering with a magnetic semiconductor can lead to nearly 100% spin injection [5]. However, at the present stage spin-dependent properties of most magnetic semiconductors are limited by the low temperature regime only, which strongly restricts their device application. Ferromagnetic metal contacts possess a much higher Curie temperature and are more attractive for application in room temperature spintronic devices. But, in conventional ohmic metal/semiconductor contacts a large conductance mismatch [6] prevents efficient injection of spin-polarized carriers. One of the solutions to this problem is to utilize a tunnelling barrier to increase interface resistance between a ferromagnetic metal source and a semiconductor structure [7, 8]. This has been demonstrated experimentally in several different designs [9–11]. Among these designs, the Schottky contact attracts more attention for several reasons. Firstly, the barrier naturally appears at the metal/semiconductor interface [12]. Secondly, it can be easily modified by an interface doping layer to increase the tunnelling current. Additionally, spin-polarized electrons

[3] Current address: Department of Physics, University of California San Diego, La Jolla, CA 92093-0360, USA.

 © 2006 IOP Publishing Ltd Printed in the UK

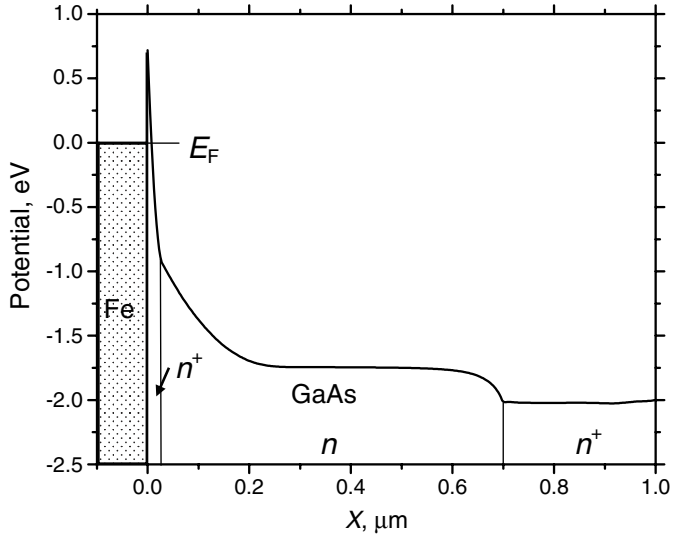

Figure 1. The potential profile together with the doping profile of the simulated structure at $T = 4.2$ K and $V_{\text{bias}} = 2$ V.

can be injected into a semiconductor up to room temperature [10, 13], and a device structure can be scaled down to the size of modern electronic devices.

Several different theoretical models have been utilized lately to describe spin injection through a Schottky barrier [7, 8, 14, 15]. However, most of these approaches are based on the assumption of quasi-equilibrium transport. Using an ensemble Monte Carlo simulation method [15], we have demonstrated that near the Schottky barrier, charge and spin dynamics of electrons are far from equilibrium. A strong electric field at the interface leads to redistribution of electrons among several valleys of conduction band in the vicinity of the barrier. Due to the coupling of electron spin with its spatial motion (spin–orbital coupling) [16], spin polarization in the semiconductor dissipates very rapidly on a deep submicron length scale that is several times shorter than the energy relaxation length. The spin scattering lengths are different in the valleys of different symmetries.

2. Model

The device modelled is a spin Schottky diode of 1 μm length that consists of a ferromagnetic metal contact and a semiconductor channel. The semiconductor channel is modulated-doped. The doping profile together with the simulated potential profile for a reverse bias $V_{\text{bias}} = 2$ V is shown in figure 1. The 30 nm n^+-layer of the channel at the interface reduces the width of the Schottky barrier and increases the efficiency of electron tunnelling from the ferromagnetic source. On the right side of the device, a highly doped layer of 250 nm width is used to produce an ohmic contact at the drain electrode. The remaining part of the channel is homogeneously n-doped. The doping concentration is equal to 2.5×10^{18} cm^{-3} and 2.5×10^{16} cm^{-3} in the n^+ and n regions, respectively. The magnetization of the ferromagnetic contact is assumed orthogonal to the metal/semiconductor interface. Such a structure can be considered as a simplification of an existing spintronic device, spin-light-emitting diode (spin-LED) [17]. We emphasize that the simplified structure is chosen to address spin dynamics near the Schottky barrier rather than

functionality of a spin-LED. The latter is more complex and should include electron capture in the quantum well and exciton recombination processes. We use Fe as the source contact of spin-polarized electrons and GaAs as the device channel. These materials are widely utilized in spintronic studies [1]. The Schottky barrier height in this case is taken as $V_B = 0.72$ eV [18].

To simulate transport properties, we utilize the ensemble Monte Carlo simulation approach [19]. It is a powerful tool that can account for details of a device structure and address transport properties in different regimes. It has been successfully applied to study hot electron transport in bulk GaAs [20]. The approach has also been used to study the tunnelling phenomenon in ballistic electron emission microscopy [21] and also in Schottky contacts [22, 15, 23].

In the model, we consider electron transport in the three non-equivalent valleys (Γ, L and X), where electron interactions with impurities, acoustic phonons and optic polar phonons are taken into consideration for intra-valley scattering and interaction with optic non-polar phonons for inter-valley scattering [24]. Other conventional details of the approach can be found in [19]. Here we focus on some assumptions used for the simulation of tunnelling through the barrier and electron spin dynamics in the valleys.

In general, to describe spin injection from a ferromagnetic metal into a non-magnetic semiconductor, one has to start with first-principle models [25]. The difficulty is that the metal conduction band structure is very complex [26], and the effective mass approximation [27], used for semiconductors, should be applied with much caution to avoid non-realistic results. Within single particle approximation, the tunnelling current density from a metal contact into a semiconductor is [28]

$$j = \frac{q g_\sigma}{(2\pi)^3} \int f_m(E)(1 - f_s(E)) v_x T(E)\, \mathrm{d}^3 k, \tag{1}$$

where q is an electron charge, g_σ accounts for spin degeneracy, E is the electron energy, v_x is the x-component of the electron velocity, $f_m(E)$ and $f_s(E)$ are distribution functions in the metal and semiconductor respectively, and $T(E)$ is the transmission coefficient. Integration is taken over the components of the electron wavevector, $\mathbf{k}$. The transmission coefficient, $T(E)$, in equation (1) accounts for matching of materials at the metal/semiconductor interface and also for tunnelling through the potential barrier [12] inside the semiconductor. There is no good analytical model for electron transmission through the ferromagnetic metal/semiconductor interface. Therefore, we try to separate its effect from the barrier tunnelling. Firstly, we assume that only the majority electrons can be injected through the interface into the semiconductor. Electrons from the Δ_1 conduction band of the ferromagnetic iron (for the band structure see [26]) can penetrate into a semiconductor for a much longer distance than other bands [25] because of the better matching on the interface. The minority conduction band of Δ_1 symmetry is far above the barrier, and its contribution to spin injection is negligible. The next assumption is that the transmission coefficient through the material interface can be factorized from the barrier tunnelling coefficient which is described by the WKB approximation [29]. The total tunnelling coefficient can therefore be written as

$$T(E) = T_{\mathrm{int}1} \mathrm{e}^{-\frac{2\sqrt{2m^*}}{\hbar} \int_0^X \sqrt{V_B(x) - E_x}\, \mathrm{d}x} T_{\mathrm{int}2}, \tag{2}$$

where m^* is the electron effective mass in the semiconductor, and $V_B(x)$ is the barrier profile. $T_{\mathrm{int}1}$ and $T_{\mathrm{int}2}$ account for metal/semiconductor and semiconductor/semiconductor interfaces of the barrier, respectively. It can be shown easily that equation (2) is exact for a thick rectangular barrier [25]. One can try to account for the interface transmission coefficient $T_{\mathrm{int}1}$ using different energy dispersion relations and different electron masses in metal and semiconductor parts [14]. However, we make further simplifications and assume that $T_{\mathrm{int}1}$ is constant within

the energy range where tunnelling through the barrier is most efficient, and T_{int2} is close to one according to the WKB approximation. In this case, interface transmission coefficient, T_{int1}, can be moved out of the integral in equation (1). Using the parabolic energy dispersion relation in the distribution function, $f_{\mathrm{m}}(E)$, and neglecting $f_{\mathrm{s}}(E)$, one can rewrite equation (1) as

$$j = \frac{A^*_\sigma T}{k_{\mathrm{B}}} \int_{-E_{\mathrm{F}}}^{\infty} T(E_x) \ln\left(1 + \mathrm{e}^{-\frac{E_x}{k_{\mathrm{B}}T}}\right) \mathrm{d}E_x, \tag{3}$$

where A^*_σ is the modified Richardson constant, k_{B} is the Boltzmann constant, T is the lattice temperature, E_x is the x-component of electron energy with respect to the Fermi level E_{F}, and $T(E_x)$ is the tunnelling coefficient. Equation (3) is similar to the standard formula utilized in electronics [12], however, it accounts for the Fermi–Dirac electron energy distribution in the metal contact. The conventional Richardson constant [12] should be corrected to include spin non-degeneracy and the interface transmission coefficient T_{int1}. With equation (3), tunnelling injection through the Schottky barrier can be efficiently modelled using the Monte Carlo method [22, 15, 23]. We have expanded the method described in [15] to account for the important aspects of 3D injection. For a given potential profile, the energy distribution of electrons tunnelled into the semiconductor during the time interval Δt is calculated using equation (3). We assume that the tunnelling barrier is one dimensional, and therefore, it affects only the x-component of the electron energy. The initial states of the successfully tunnelled electrons are generated based on the Fermi–Dirac energy distribution on the metal side of the barrier. In both, metal and semiconductor, energy dispersion relations are assumed to be parabolic. The spin state of the electrons injected is conserved during the tunnelling and starts to evolve under the influence of a spin-dependent Hamiltonian during the drift motion in the semiconductor channel of the device.

To describe the spin dynamics of injected electrons, we take into account the spin–orbit coupling due to the inversion asymmetry of GaAs crystal [16]. This interaction, together with electron momentum scattering events, produces rotational spin dephasing in a system of spin-polarized electrons [30]. In the model, it is implemented as the spin rotation of each electron in the driving field during the electron free propagation between two scattering events. The initial states of electrons are obtained from the injection procedure. The profile of the Schottky barrier is determined by the self-consistent solution of charge carrier motion and the Poisson equation. To describe the spin of a single electron, we use a single electron spin density matrix [31, 32] representation that is equivalent to the spin polarization vector description [33, 34]. Details of the simulation procedure applied for spin transport in low dimensional structures can be found in [31]. For the electron wavevector in the vicinity of points of high symmetry within the Brillouin zone, an analytical form for corrections to the effective mass Hamiltonian due to the spin–orbit interaction has been derived in [16]. Near the bottom of the valleys, the spin–orbit Hamiltonians can be written in the following form [35]

$$H_\Gamma = \alpha_\Gamma(k_x\sigma_x(k_y^2 - k_z^2) + k_y\sigma_y(k_z^2 - k_x^2) + k_z\sigma_z(k_x^2 - k_y^2)) \tag{4}$$

in the Γ-valley,

$$H_{\mathrm{L}} = \alpha_{\mathrm{L}}/\sqrt{3}(\sigma_x(k_y - k_z) + \sigma_y(k_z - k_x) + \sigma_z(k_x - k_y)) \tag{5}$$

in the L-valley located along the [111] direction in the crystallographic axes, and

$$H_{\mathrm{X}} = \alpha_{\mathrm{X}}(\sigma_z k_z - \sigma_y k_y) \tag{6}$$

in the X-valley located along the [100] direction. In equations (4)–(6), σ_α are the spin Pauli matrices [29], k_α the components of an electron wavevector, and α_Γ, α_{L} and α_{X} the spin–orbital coupling coefficients. Explicit forms of spin–orbit Hamiltonians for other equivalent valleys of L and X symmetries can be obtained by appropriate rotation of the coordinate system. In the

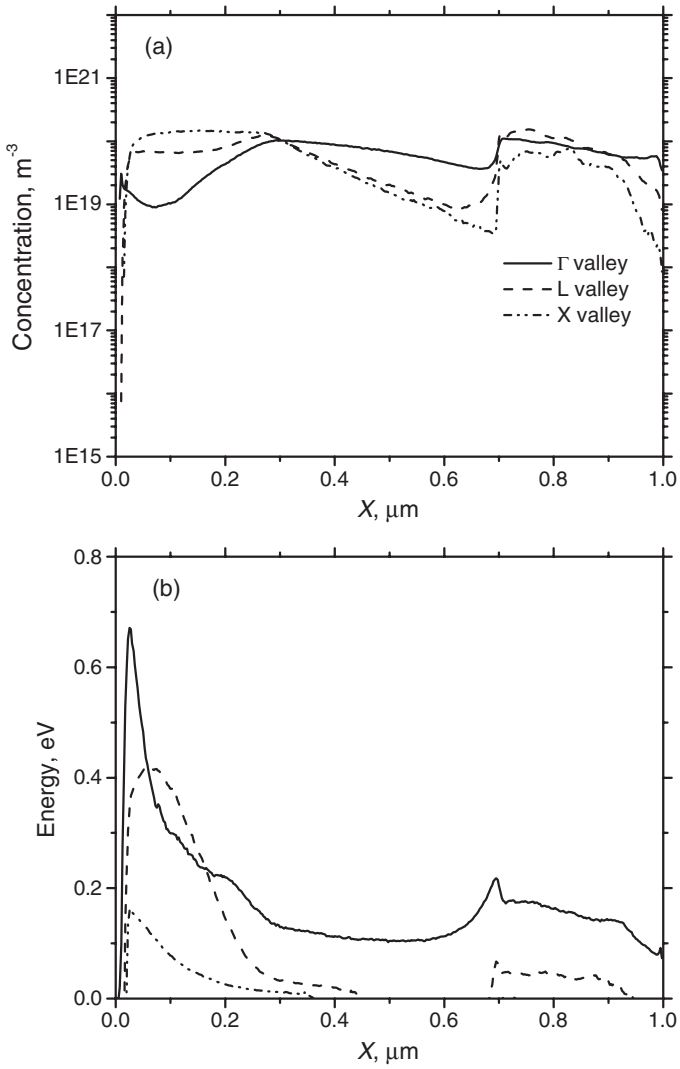

Figure 2. Populations of electrons in different valleys injected into the device (a), average energies of injected electrons (b) at $T = 4.2$ K, and $V_{\text{bias}} = 2$ V.

model, we assume that one of the appropriate equations in equtions (4)–(6) can be applied to the electrons in a given valley. However, it should be noted that these equations are correct only near the bottoms of the valleys. The spin–orbit coupling coefficients utilized in simulations are $\alpha_\Gamma = 28$ eV Å^3 [36], $\alpha_L = 0.27$ eV Å [37], and $\alpha_X = 0.087$ eV Å [36]. We would like to emphasize that due to a lack of information on spin coupling parameters in the upper valleys their actual values may be different.

3. Simulation results and discussion

We simulated steady-state injection of spin-polarized electrons into the device shown in figure 1 for $T = 4.2$–350 K, and $V_{\text{bias}} = 1$–3 V. The concentration and average energy profiles of electrons injected at $T = 4.2$ K and $V_{\text{bias}} = 2$ V are shown in figures 2(a) and (b).

Near the metal/semiconductor interface, electrons injected into the semiconductor are strongly accelerated by the interface electric field. At a distance of about 20–30 nm from the interface, the intervalley scattering mechanism becomes dominant, and electrons are redistributed among the valleys. As demonstrated in previous studies [20], the electron population becomes even higher in the upper valleys than in the Γ-valley. Scattering of electrons back to the Γ-valley becomes evident after travelling for a distance of the order of several hundred nanometres. These profiles remain similar for the whole ranges of voltage and temperature, though actual values of concentration and energy change. At low temperature, practically all of the electrons are injected by tunnelling near the Fermi level in the metal contact, while at temperatures of ∼50–70 K, thermal assisted tunnelling starts to play a role. The contribution of the thermionic emission becomes noticeable only at temperatures above 150 K.

To characterize spin properties of injected current, we use electron spin polarization, defined as

$$S_\alpha = \sum_i \mathrm{Tr}(\sigma_\alpha \rho_\sigma^i) \Big/ \sum_i \mathrm{Tr}(\rho_\sigma^i), \tag{7}$$

and current spin polarization

$$P_\alpha = \sum_i v_x^i \,\mathrm{Tr}(\sigma_\alpha \rho_\sigma^i) \Big/ \sum_i v_x^i \,\mathrm{Tr}(\rho_\sigma^i), \tag{8}$$

where ρ_σ^i is the single electron spin density matrix [29] and v_x^i is the x-component of velocity of the ith particle. In equations (7) and (8), sums are taken over all the injected particles located within a small volume d^3x near the position $\boldsymbol{x}$. Equations (7) and (8) are similar to the standard definitions of particle and flux polarization utilized in the literature [1, 38]. In general, electron spin polarization is easier to measure experimentally, for example, using the oblique Hanle effect [11]. However, in a device, electrons injected represent only a small fraction of the total number of carriers. In the structure studied, see figure 1, total electron spin polarization is negligible except for the depletion region. Current spin polarization, equation (8), by definition, cancels the effect of background electrons in the device channel that do not contribute to the current. However, it is not clear how this characteristic can be measured. One of the possible methods is discussed in [39].

In simulations, we observe that both characteristics of spin polarization decay very rapidly in a length scale of the order of 50–100 nm. Simulated profiles at $T = 4.2$ K and $V_{\mathrm{bias}} = 2$ V are shown in figure 3. Spin dynamics, controlled by spin–orbit coupling, equations (4)–(6), and electron momentum distributions are different in different valleys. With the given set of transport parameters, we find that spin characteristics in the upper valleys decay about twice as fast as those in the Γ-valley for the temperature and applied bias ranges, $T = 4.2$–350 K and $V_{\mathrm{bias}} = 1$–3 V. In the Γ-valley, both electron and current spin polarization profiles can be fitted by $\exp(-(x/x_0)^\alpha)$, where coefficient $\alpha \sim 2$–3, rather than by the linear exponential decay function with $\alpha = 1$. This dependence cannot be explained within the drift-diffusion approximation [38, 40]. To characterize spin dephasing, we use electron and current spin scattering lengths which are defined as the lengths where electron spin and current spin polarizations decay to $1/e$ of their initial values, respectively. With the temperature increment, both spin scattering lengths decrease monotonically, see figure 4. At room temperature, spin scattering lengths in the Γ-valley are more than two times shorter than at $T = 4.2$ K. Evident bias voltage dependence of spin scattering lengths is observed for electrons in the Γ-valley only, see figure 5. Similarly to the studies using drift-diffusion models [38, 41, 40], our results show that at higher bias, electron spin polarization penetrates more deeply into the semiconductor. However, this dependence is weak. For the current spin scattering length, we observe a reverse tendency. It becomes shorter at higher bias.

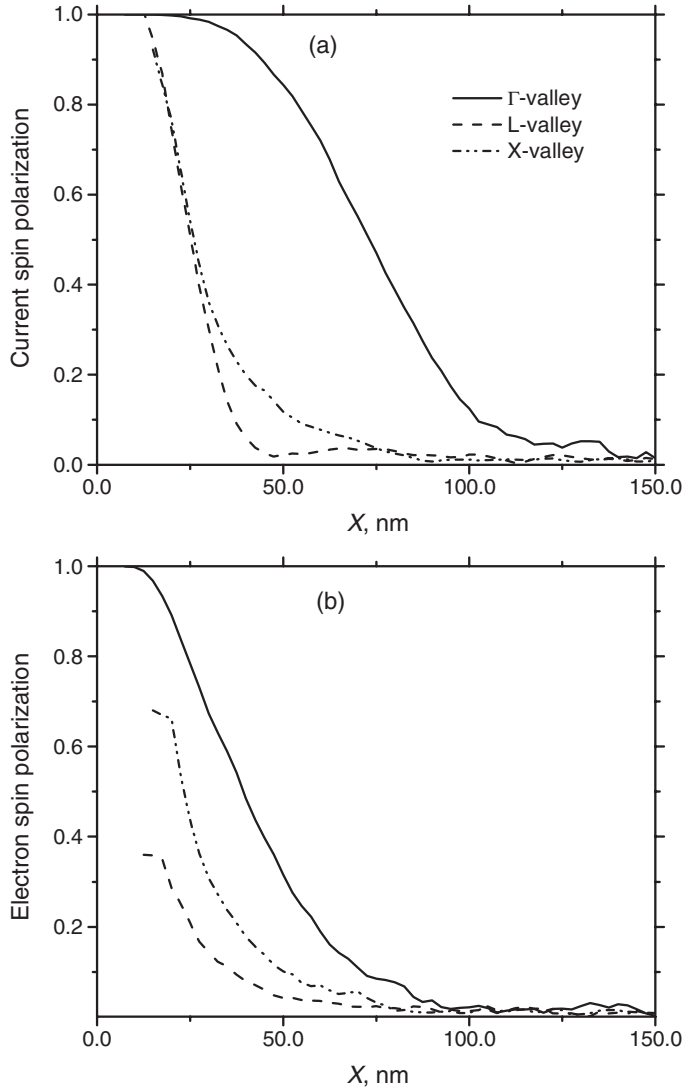

Figure 3. Current spin polarization profile (a), and electron spin polarization profile (b) simulated at $T = 4.2$ K and $V_{\text{bias}} = 2$ V.

Signatures of hot spin-polarized carrier transport in structures with Schottky barriers have been observed recently [42]. Our simulations confirm that spin-polarized transport can be detected in spin-LED structures. In a more detailed comparison of simulated results with experimental data on spin injection in spin-LEDs, we find that the model provides qualitatively consistent spin scattering length scales with some overestimation of the spin dephasing effect. The latter can be due to different setups in the simulations and experimental study, and also due to not well matched transport parameters. Transport parameters within the range accessible in the literature give variations in electron and current spin scattering lengths of the order of 10–15%. The most crucial are spin–orbit coupling coefficients. For the L and X valleys, only theoretical estimations [36, 37] are available. For the Γ-valley, the measured value of spin–orbit

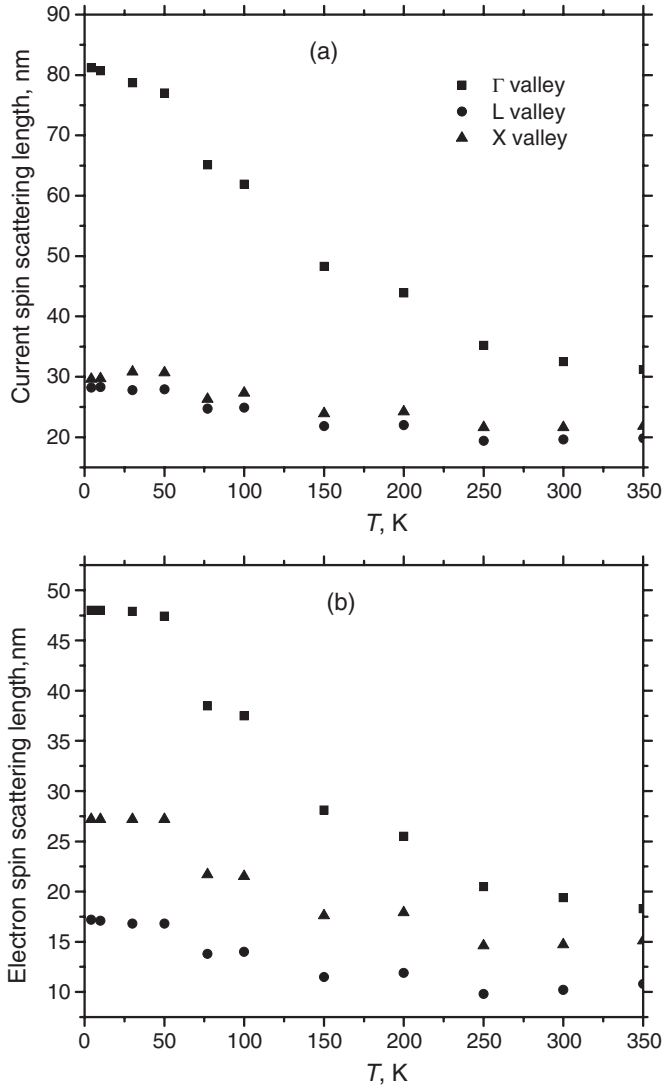

Figure 4. Temperature dependences of current spin scattering length (a), and electron spin scattering length (b) at $V_{\text{bias}} = 2$ V.

coupling coefficient corresponds to its minimum. However, in the simulations, electrons in this valley possess high kinetic energy, see figure 2(b). In this case, the coupling coefficient should be modified. We have also accounted for spin rotation in a homogeneous external magnetic field that is utilized in experiments with spin-LEDs. For simplicity we used isotropic g-factors $g^*_\Gamma = -0.44$ [43], $g^*_{\text{L}} = 2$ [44], and $g^*_{\text{X}} = 2$. However, we found that the effect is negligible for magnetic fields up to $H = 2$ T.

4. Conclusion

In conclusion, we simulated injection of spin-polarized electrons through a Schottky barrier into a GaAs device channel. For the whole temperature range, $T = 4.2$–350 K, and the

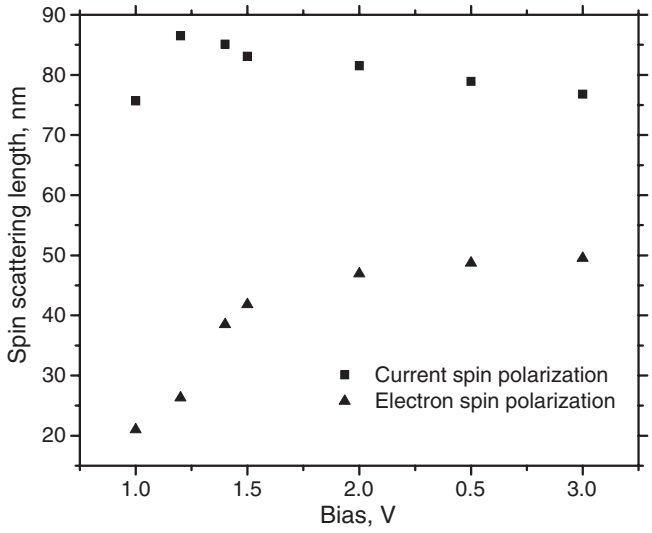

Figure 5. Current spin and electron spin scattering lengths in the Γ-valley as functions of applied bias at $T = 4.2$ K.

applied bias range, $V_{\text{bias}} = 1$–3 V, we observed hot-electron transport features. Electrons injected through the barrier quickly redistributed among the semiconductor valleys. On the length scale of the order of 200–300 nm from the metal/semiconductor interface, upper valleys (X and L) are more populated by the injected electrons than the Γ-valley. Electron and current spin polarizations injected decay in a very short length scale of the order of 50–100 nm. Within the model developed, spin polarization characteristics decay faster in the upper valleys.

Acknowledgments

We are grateful to Robert Mallory, Athos Petrou, Vladimir Privman and Mesut Yasar for useful discussions. The research was supported by the National Science Foundation, grant DMR-0121146. The work of SS is also supported by DMR-0403465.

References

[1] Zutic I, Fabian J and Das Sarma S 2004 Spintronics: fundamentals and applications *Rev. Mod. Phys.* **76** 323
[2] Jonker B T 2003 Progress toward electrical injection of spin-polarized electrons into semiconductors *Proc. IEEE* **91** 727
[3] Ploog K H 2002 Spin injection in ferromagnet–semiconductor heterostructures at room temperature *J. Appl. Phys.* **91** 7256
[4] Fiederling R, Keim M, Reuscher G, Ossau W, Schmidt G, Waag A and Molenkamp L W 1999 *Nature* **402** 787
[5] Egues J C 1998 Spin-dependent perpendicular magnetotransport through a tunable ZnSe/$Zn_{1-x}Mn_xSe$ heterostructure: a possible spin filter? *Phys. Rev. Lett.* **80** 4578
[6] Schmidt G, Ferrand D, Molenkamp L W, Filip A T and van Wees B J 2000 Fundamental obstacle for electrical spin injection from a ferromagnetic metal into a diffusive semiconductor *Phys. Rev.* B **62** R4790
[7] Rashba E I 2000 Theory of electrical spin injection: tunnel contacts as a solution of the conductivity mismatch problem *Phys. Rev.* B **62** R16267
[8] Albrecht J D and Smith D L 2003 Spin-polarized electron transport at ferromagnet/semiconductor Schottky contacts *Phys. Rev.* B **68** 035340
[9] Alvarado S F and Renaud P 1992 Observation of spin-polarized-electron tunnelling from a ferromagnet into GaAs *Phys. Rev. Lett.* **68** 1387
[10] Hanbicki A T, Jonker B T, Itskos G, Kioseoglou G and Petrou A 2002 Efficient electrical spin injection from a magnetic metal/tunnelling barrier contact into a semiconductor *Appl. Phys. Lett.* **80** 1240

[11] Motsnyi V F, Van Dorpe P, Van Roy W, Goovaerts E, Safarov V I, Borghs G and De Boeck J 2003 Optical investigation of electrical spin injection into semiconductors *Phys. Rev.* B **68** 245319
[12] Sze S M 1981 *Physics of Semiconductor Devices* (New York: Wiley)
[13] Adelmann C, Lou X, Strand J, Palmstrom C J and Crowell P A 2005 Spin injection and relaxation in ferromagnet–semiconductor heterostructures *Phys. Rev.* B **71** 121301(R)
[14] Osipov V V and Bratkovsky A M 2004 Efficient nonlinear room-temperature spin injection from ferromagnets into semiconductors through a modified Schottky barrier *Phys. Rev.* B **70** 205312
[15] Shen M, Saikin S and Cheng M-C 2004 Monte Carlo modeling of spin injection through a Schottky barrier and spin transport in a semiconductor quantum well *J. Appl. Phys.* **96** 4319
[16] Dresselhaus G 1955 Spin–orbit coupling effects in zinc blende structures *Phys. Rev.* **100** 580
[17] Hanbicki A T, van t Erve O M J, Magno R, Kioseoglou G, Li C H, Jonker B T, Itskos G, Mallory R, Yasar M and Petrou A 2003 Analysis of the transport process providing spin injection through an Fe/AlGaAs Schottky barrier *Appl. Phys. Lett.* **82** 4092
[18] Waldrop J R 1984 Schottky-barrier height of ideal metal contact to GaAs *Appl. Phys. Lett.* **44** 1002
[19] Moglestue C 1993 *Monte Carlo Simulation of Semiconductor Devices* (New York: Chapman and Hall)
[20] Pozela J and Reklaitis A 1980 Electron transport properties in GaAs at high electric fields *Solid State Electron.* **23** 927
[21] Appelbaum I and Narayanamurti V 2005 Monte Carlo calculations for metal–semiconductor hot-electron injection via tunnel-junction emission *Phys. Rev.* B **71** 045320
[22] Sun L, Liu X Y, Liu M, Du G and Han R Q 2003 Monte Carlo simulation of Schottky contact with direct tunnelling model *Semicond. Sci. Technol.* **18** 576
[23] Wang Y Y and Wu M W 2005 Schottky-barrier induced spin dephasing in spin injection *Phys. Rev.* B **72** 153301
[24] For scattering formulas see Fischetti M V and Laux S E 1995 *DAMOCLES Theoretical Manual* IBM Research Division, Yorktown heights
[25] Zhang X-G and Butler W H 2003 Band structure, evanescent states, and transport in spin tunnel junctions *J. Phys.: Condens. Matter* **15** R1603
[26] Callaway J and Wang C S 1977 Energy bands in ferromagnetic iron *Phys. Rev.* B **16** 2095
[27] Kohn W 1957 Effective mass theory in solids from a many-particle standpoint *Phys. Rev.* **105** 509
[28] Duke C B 1969 Theory of metal–barrier–metal tunnelling *Tunneling Phenomena in Solids* (New York: Plenum)
[29] Merzbacher E 2004 *Quantum Mechanics* (New York: Wiley)
[30] Dyakonov M I and Perel V I 1971 Spin orientation of electrons associated with the interband absorption of light in semiconductors *Sov. Phys.—JETP* **33** 1053
[31] Saikin S, Shen M, Cheng M-C and Privman V 2003 Semiclassical Monte-Carlo model for in-plane transport of spin-polarized electrons in III–V heterostructures *J. Appl. Phys.* **94** 1769
[32] Pramanik S, Bandyopadhyay S and Cahay M 2003 Spin dephasing in quantum wires *Phys. Rev.* B **68** 075313
[33] Kiselev A A and Kim K W 2000 Progressive suppression of spin relaxation in two-dimensional channels of finite width *Phys. Rev.* B **61** 13115
[34] Pershin Y V and Privman V 2004 Slow spin relaxation in two-dimensional electron systems with antidotes *Phys. Rev.* B **69** 073310
[35] Ivchenko E L and Pikus G E 1997 Superlattices and other heterostructures. Symmetry and optical phenomena *Solid-State Sciences* vol 110 (Berlin: Springer)
[36] Cardona M, Christensen N E and Fasol G 1988 Relativistic band structure and spin–orbit splitting of zinc-blende-type semiconductors *Phys. Rev.* B **38** 1806
[37] Jancu J-M, Scholz R, La Rocca G C, de Andrada e Silva E A and Voisin P 2004 Giant spin splittings in GaSb/AlSb L-valley quantum well *Phys. Rev.* B **70** 121306(R)
[38] Yu Z G and Flatte M E 2002 Spin diffusion and injection in semiconductor structures: electric field effects *Phys. Rev.* B **66** 235302
[39] Di Lorenzo A and Nazarov Y V 2004 Full counting statistics of spin currents *Phys. Rev. Lett.* **93** 046601
[40] Saikin S 2004 Drift-diffusion model for spin-polarized transport in a non-degenerate 2DEG controlled by a spin–orbit interaction *J. Phys.: Condens. Matter* **16** 5071
[41] Zutic I, Fabian J and Das Sarma S 2002 Spin-polarized transport in inhomogeneous magnetic semiconductors: theory of magnetic/nonmagnetic p–n junctions *Phys. Rev. Lett.* **88** 066603
[42] Mallory R, Yasar M, Itskos G, Petrou A, Kioseoglou G, Hanbicki A T, Li C H, van 't Erve O M J, Jonker B T, Shen M and Saikin S 2005 *Preprint*
[43] Madelung O 1996 *Semiconductors—Basic Data* (Berlin: Springer)
[44] Baron F A, Kiselev A A, Robinson H D, Kim K W, Wang K L and Yablonovitch E 2003 Manipulating the L-valley electron g factor in Si–Ge heterostructures *Phys. Rev.* B **68** 195306